Proceedings of Engineering and Technology Innovation, vol. 24, 2023, pp. 41-52

Forward Kinematics Based Prediction for Bending Motion of Soft Pneumatic Actuators with Various Air Chambers

Do Phuoc Thien[1,2], Le Hoai Phuong[1,2,*]

[1]Industrial Maintenance Training Center, Ho Chi Minh City University of Technology, Ho Chi Minh City, Vietnam

[2]Vietnam National University Ho Chi Minh City, Ho Chi Minh City, Vietnam

Received 04 August 2022; received in revised form 23 October 2022; accepted 09 November 2022

DOI: https://doi.org/10.46604/peti.2023.10536

Abstract

This study proposes a forward kinematic model for soft actuators that utilize pneumatic control to predict their bending motion, which is simulated using Ansys software. Firstly, a bending motion test is conducted with a 2-air chamber actuator to derive an equation that establishes the relationship between the bending angle and input pressure. Next, a serial model for the overall soft actuator is developed using forward kinematics with the DH method. The angle variables in the soft actuator are then replaced with an equation that relates the deformed angle and compressed air. Finally, the proposed serial model is used to predict the bending motion of 4-air and 6-air chamber actuators, and the results are compared to simulations and real experiments. The comparison shows that the proposed model could accurately predict the bending motion of the real actuators within an acceptable tolerance of 10%.

Keywords: soft robotic, pneumatic actuator, forward kinematics, flexible finger, DH parameter

1. Introduction

Recent years have seen a growing interest among researchers in soft robotics due to its wide-ranging potential applications [1]. Soft robotics technology has the potential to revolutionize how we design and control robots, particularly regarding safety mechanisms for human interaction. However, significant challenges must be addressed to fully utilize this technology's potential. These challenges include further research, improved designs and models, and more sophisticated control mechanisms for these remarkable machines [2]. Soft actuators can be easily fabricated using casting or 3D printing techniques [3-4]. Despite their softness, they can generate high forces, making them suitable for various applications [5]. The soft robot possesses a pliable structure and limitless degrees of freedom, making it capable of simultaneously bending and stretching in various directions.

Furthermore, it is well-suited for performing in intricate work environments [6]. Currently, there are several research fields in the area of soft robotics. These include the development of a flexible robotic arm [7], the design of an assisted robot for rehabilitation that employs soft pneumatic actuators [3], the creation of a dual-mode soft gripper using silicone material [8], and the use of soft robotics in surgical applications [9]. Various methods have been developed to solve the displacement of a soft actuator, including the derivation of Lagrangian dynamic equations. Wang and Hirai [10] experimented with fluidic elastomer actuators fabricated using 3D printing. They observed the bending angles of a single actuator under various pressures to demonstrate the repeatability of the actuation process. They then proposed a dynamic model that accurately replicated the deformation motion of the fluidic elastomer actuator.

* Corresponding author. E-mail address: lhphuong@hcmut.edu.vn

Al-Fahaam et al. [11] proposed a geometry-based approach for computing the motion of soft robots using an optimization problem to determine the controller and actuator as geometrical elements. Their framework efficiently computes soft manipulators' forward and inverse kinematics with low computational costs, even for components with multiple materials. Luo et al. [12] and Salem et al. [13] presented spline-based models and control frameworks for soft robotics, utilizing heterogeneous rational B-splines to capture material and physical properties while preserving the dynamics with environmental interactions. The dynamic model based on non-uniform rational B-spline (NURBS) allows for optimal control design using predictive control with a finite number of control points, reducing the motion control of the infinite-dimensional soft body.

The study of forward kinematics (FK) is a crucial topic covered in many educational resources. One widely used approach for describing the kinematic relationships between the links in a chain of rigid rods connected by lower pair joints with one degree of freedom (such as rotational and prismatic joints) is the Denavit-Hartenberg (DH) convention [14]. This convention provides a concise and consistent representation of the robot's kinematic structure and is widely used in the field. It offers a minimal description and a straightforward solution for parameter verification. Additionally, the DH convention relies on linear algebra, which allows for efficient matrix computations [15].

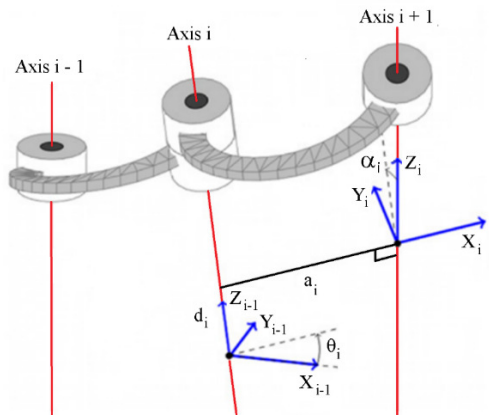

Fig. 1 DH parameters [14]

This study presents the use of FK to model the movement of a soft pneumatic actuator with two contiguous air chambers. The experiments are conducted on a 2-air chamber actuator, and the FK is then utilized to predict the bending motion of the soft pneumatic actuators with different numbers of air chambers. The DH parameters are used to calculate the transformation matrices, as illustrated in Fig. 1. Since the soft pneumatic actuators rotate only around and do not have any movements along the z-axis, it is straightforward to obtain the transformation matrices.

2. The Conceptual Design and Fabrication Process

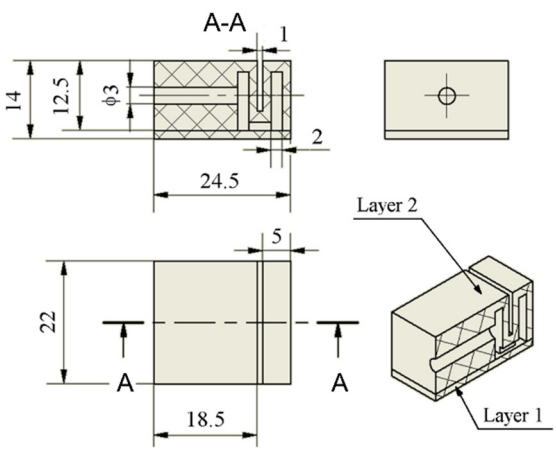

Fig. 2 The dimension of the soft pneumatic finger (mm)

The pneumatic networks (PneuNets) bending actuator is used as the design of the soft pneumatic actuator of this study. It consists of two air chambers with identical dimensions, an air chamber layer, and a bottom layer. The air chamber has a wall thickness of 1.5 mm, and a long inlet hole is created to fit the air-supplied tube and prevent leakage of compressed air from the actuator. The 2D design is sketched in Inventor software and presented in Fig. 2.

Furthermore, the fabrication process is illustrated in Fig. 3 and consists of three steps. Firstly, the molds for the actuator are designed using the actuator geometry and created with a 3D printing machine. Secondly, the platinum silicone is poured into the mold, cured for the required time, and then separated and glued together. Additionally, an M3 screw is utilized to create the inlet hole inside the actuator. Two molds are assembled for each layer as the actuator has two parts with different layers. Platinum silicone is used as the material for the actuator, which requires 8-10 hours to solidify.

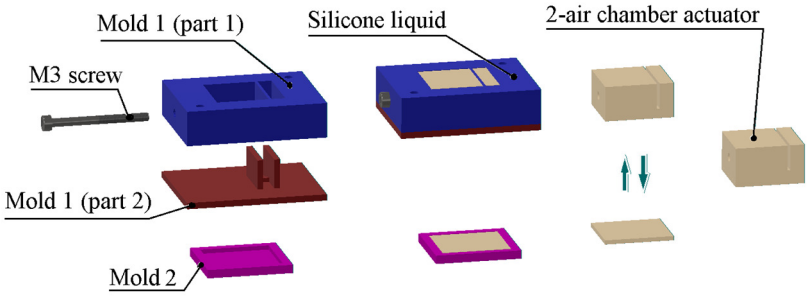

Fig. 3 The fabrication process of a 2-air chamber pneumatic actuator Finite Element Analysis

The addition of silicone diluent oil to the liquid is recommended to reduce the occurrence of bubbles during the filling process of the molds. However, in case of the appearance of bubbles, a needle can be used to prick them manually on the top and inside of the mold. It is worth noting that using the liquid does not alter the material properties, such as Young's modulus and hardness. Alternatively, a vacuum pump can also be used to remove the bubbles without affecting any material properties.

3. Finite Element Analysis (FEA)

The bending angles of the 4-air and 6-air chamber actuators are first compared through simulations. Afterward, the experiment, simulation, and prediction results of these actuators are compared. To simulate the behavior of a soft pneumatic actuator, its mechanical properties need to be verified, such as its elasticity characterized by Young's modulus. The material datasheet shows that the silicone platinum used to make soft actuators has a Shore hardness of 30, which can be converted to Young's modulus. During the tensile testing and Shore, a scale hardness measurements of the dental elastomers, Young's modulus was determined using the Gent equation [16] based on the directly obtained hardness values:

$$\mathrm{E}(\mathrm{MPa}) = \frac{0.0981 \times (5 + 7.66 \times s)}{0.137505 \times (254 - 2.54 \times s)} \tag{1}$$

where s is the Shore hardness (s = 30), Young's modulus of E = 1.16 MPa, and Poisson's ratio = 0.49.

Eq. (1) is used to convert the hardness unit from Shore A to MPa because the input data for the analysis is Young's modulus, which is typically expressed in MPa. Converting the hardness values to MPa through Eq. (1) allows for a more straightforward comparison of the mechanical properties of different materials, as they are now in the same unit of measure. In this study, the FEA method is employed to evaluate the design of the actuator structure. Due to the complexity of the soft actuator's structure, a computational model is utilized instead of a complex theoretical model. Ansys software is utilized to perform the simulations, which allowed for the determination of the bending motion of actuators before fabrication. The angles of each joint are measured, and their average values are calculated to compare them with the 2-air chamber actuator. The obtained results are illustrated in Figs. 4-5.

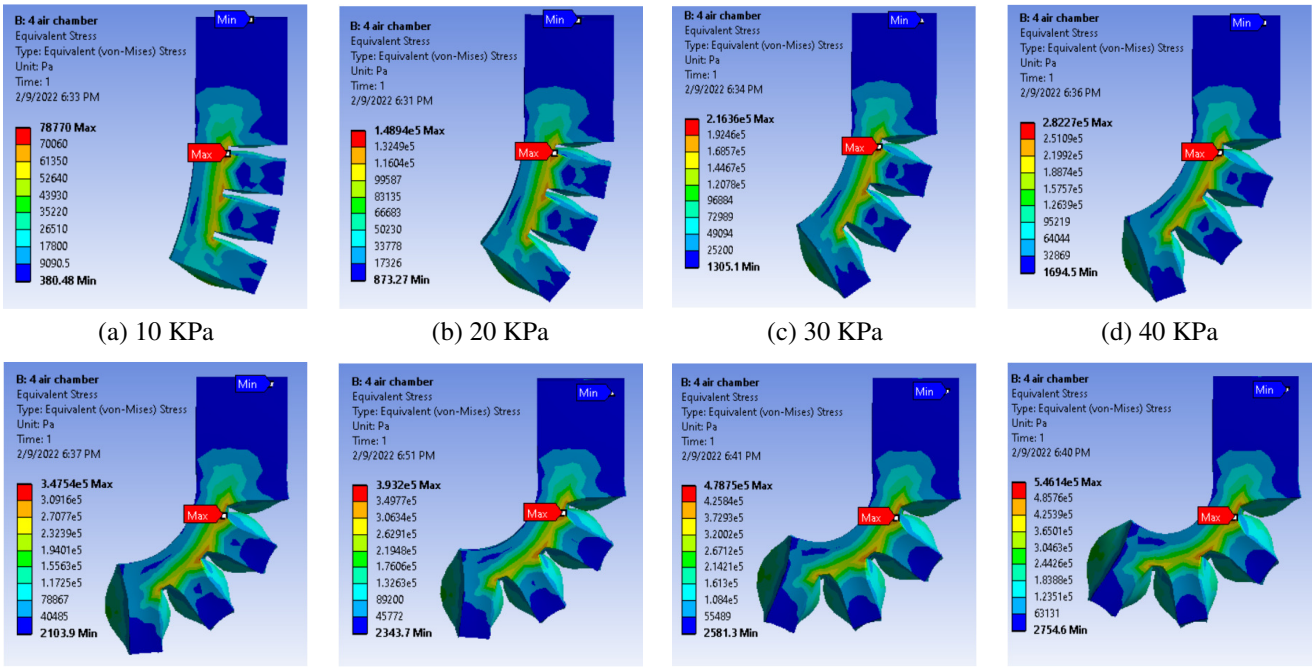

(a) 10 KPa (b) 20 KPa (c) 30 KPa (d) 40 KPa

(e) 50 KPa (f) 60 KPa (g) 70 KPa (h) 80 KPa

Fig. 4 FEA of the 4-air chamber actuator

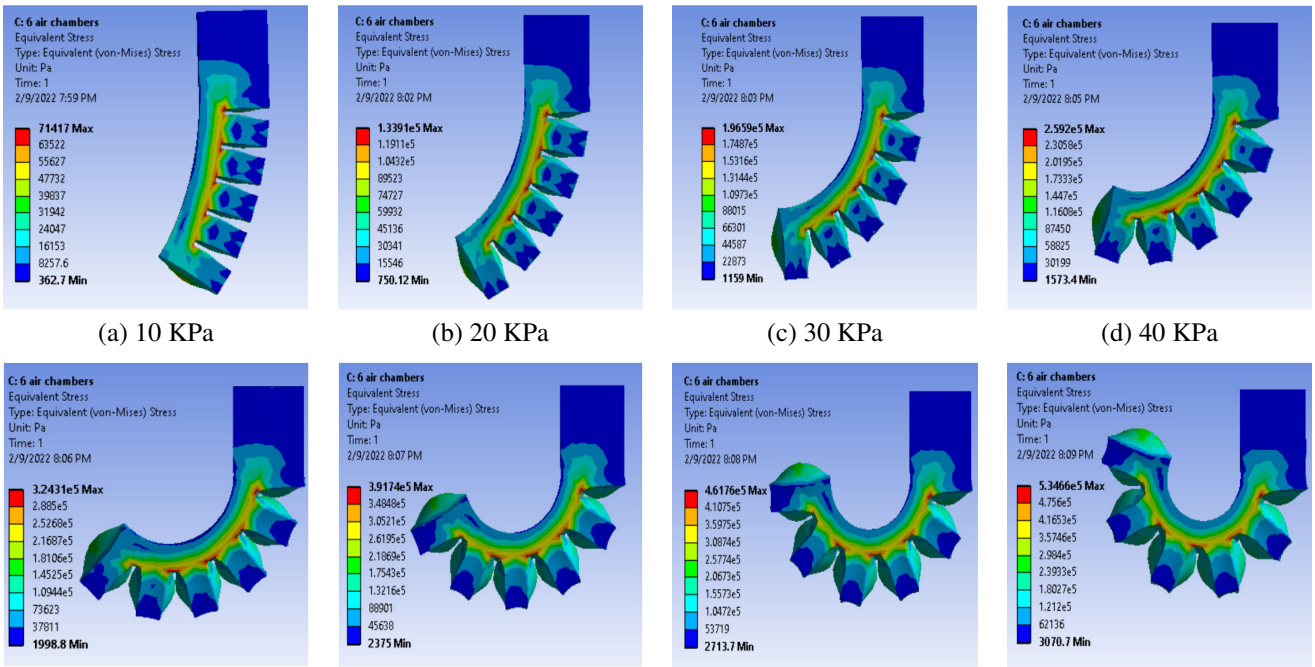

(a) 10 KPa (b) 20 KPa (c) 30 KPa (d) 40 KPa

(e) 50 KPa (f) 60 KPa (g) 70 KPa (h) 80 KPa

Fig. 5 FEA of the 6-air chamber actuator

4. Bending Angle Measurement

The bending angle experiment is conducted to determine the bending angle of a two-air chamber actuator and to derive an equation that expresses the relationship between the input air pressure and bending motion. The resulting equation is then used to predict the bending motion of the actuator with different numbers of air chambers.

4.1. 2-air chamber

This experiment measures the bending angle between two air chambers in the soft robot. To achieve this, a pressure gauge is utilized to measure compressed air, while a pair of flow control valves are used to adjust the air pressure supplied to the soft

actuators. The experimental setup diagram is shown in Fig. 6, where the soft robot is attached to a 3D-printed connector mounted in a shaft. The first flow control valve is used to supply input pressure, while the second valve is used to release the supplied pressure. By combining these two valves, the air pressure for the actuator can be controlled manually.

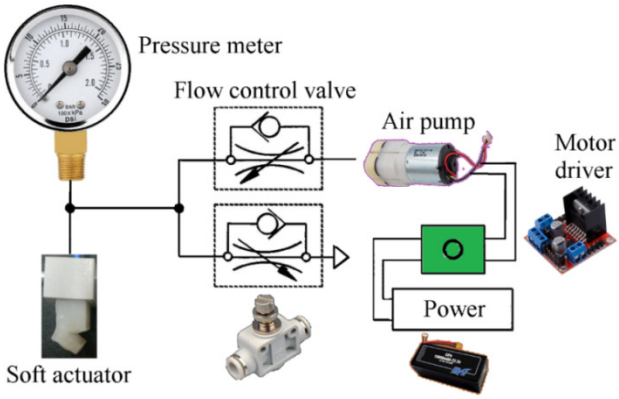

Fig. 6 The experimental setup diagram

This experiment does not utilize any integrated sensor within the actuator to determine its bending motion. Instead, a camera is employed to capture multiple images while adjusting the air pressure supplied to the soft actuators. Subsequently, the AutoCAD software is used to draw two lines and a rotational joint that overrides the curve of the bottom cover of the 2-air chamber actuator, as illustrated in Fig. 7. The bending angle is then measured directly from the images, along with the corresponding air pressure values. Since the actuator comprises two air chambers, it has two rigid links and a rotational joint. Therefore, the first link, represented by the first line, is from the reference point to the mid of the two air chambers, while the second link is from the midpoint of the two air chambers to the final point. Furthermore, the angle experiments are conducted five times and the mean value is computed from the five trials to obtain more accurate results.

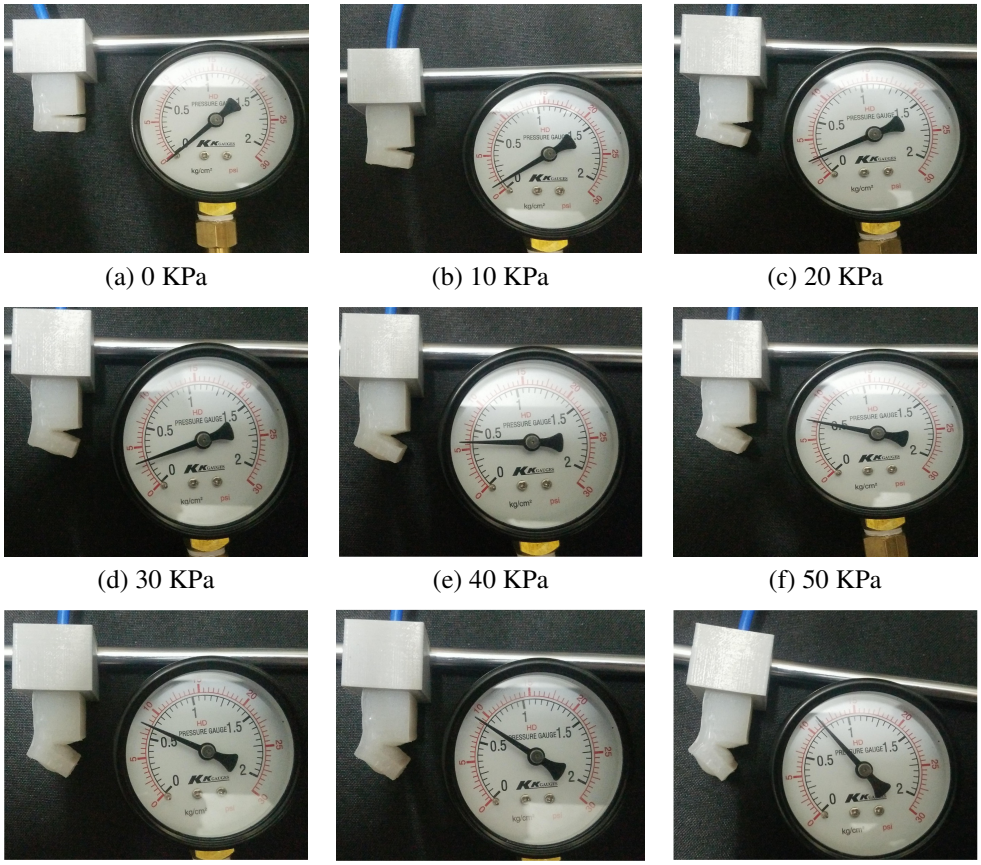

(a) 0 KPa (b) 10 KPa (c) 20 KPa

(d) 30 KPa (e) 40 KPa (f) 50 KPa

(g) 60 KPa (h) 70 KPa (i) 80 KPa

Fig. 7 Measuring the bending motion of a 2-air chamber actuator

The test results shown in Fig. 8 demonstrate that as the pressure supplied by the soft actuator increases, the actuator's deformed angle also increases. The experiment is repeated five times to obtain more accurate results, and the mean value is calculated. The collected data are graphed to display the experimental bending angle. A mathematical model is then used to interpolate the experimental data and determine the relationship between the bending angle and the compressed air pressure:

$$Bending_angle(degree) = -0.0036 \times Pressure^2 + 0.6916 \times Pressure(KPa) \tag{2}$$

The bending motion of the actuator appears to be non-linear when compressed air is supplied between 0 KPa to 80 KPa. Therefore, a quadratic equation is used for polynomial interpolation to obtain the relationship between the bending angle and compressed air, as expressed in Eq. (2). This equation can be used to predict the motion of a PneuNets actuator with two air chambers. In the subsequent part of the study, the estimated bending angle values of the PneuNets actuator with different air chamber quantities will be obtained by Eq. (2). The range of air pressure used for experimentation is between 0 KPa to 80 KPa since the air pump motor can supply compressed air up to 80 KPa.

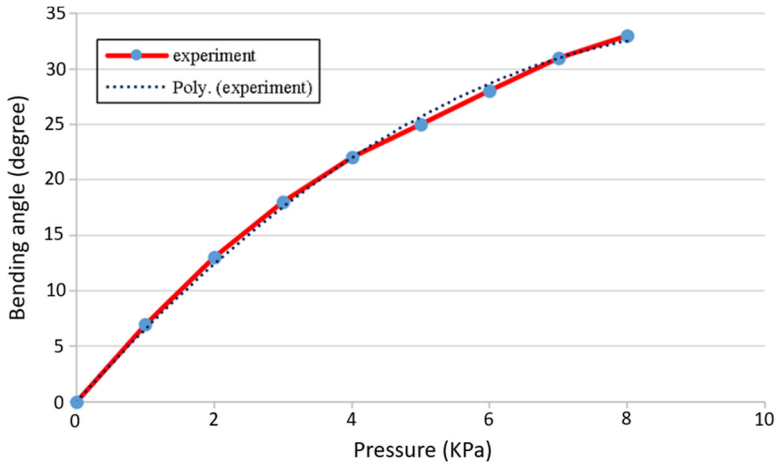

Fig. 8 The experimental result of the 2-air chamber actuator

4.2. 4-air and 6-air chambers

The experiments shown in Figs. 9-10 were carried out using a similar setup to the previous test, with five trial tests conducted. The average angle values of each joint were measured and calculated, and compared with those of the 2-air, 4-air, and 6-air chamber actuators, as well as the motion prediction. These data were used to evaluate the efficiency of the predicted formula and to compare the bending motion of the simulation, experimental tests, and prediction.

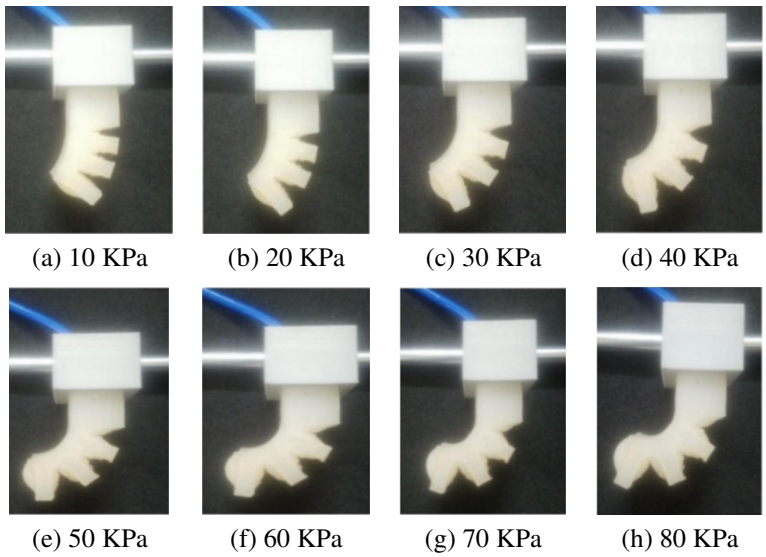

(a) 10 KPa (b) 20 KPa (c) 30 KPa (d) 40 KPa

(e) 50 KPa (f) 60 KPa (g) 70 KPa (h) 80 KPa

Fig. 9 The 4-air chamber actuator bending angle experiment

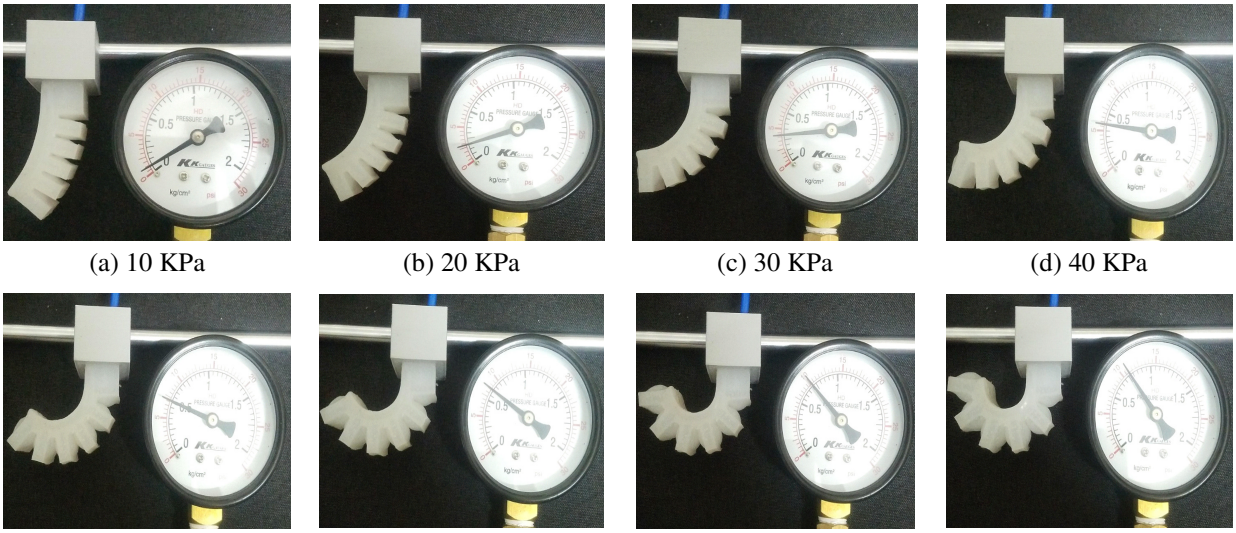

(a) 10 KPa (b) 20 KPa (c) 30 KPa (d) 40 KPa

(e) 50 KPa (f) 60 KPa (g) 70 KPa (h) 80 KPa

Fig. 10 The 6-air chamber actuator bending angle experiment

5. Actuator Modelling

When compressed air is supplied to the soft actuator, the air chambers will inflate and create a bending motion at the middle point of the two air chambers. The number of revolute joints in the model is equal to the number of air chambers minus one, as illustrated in Fig. 11.

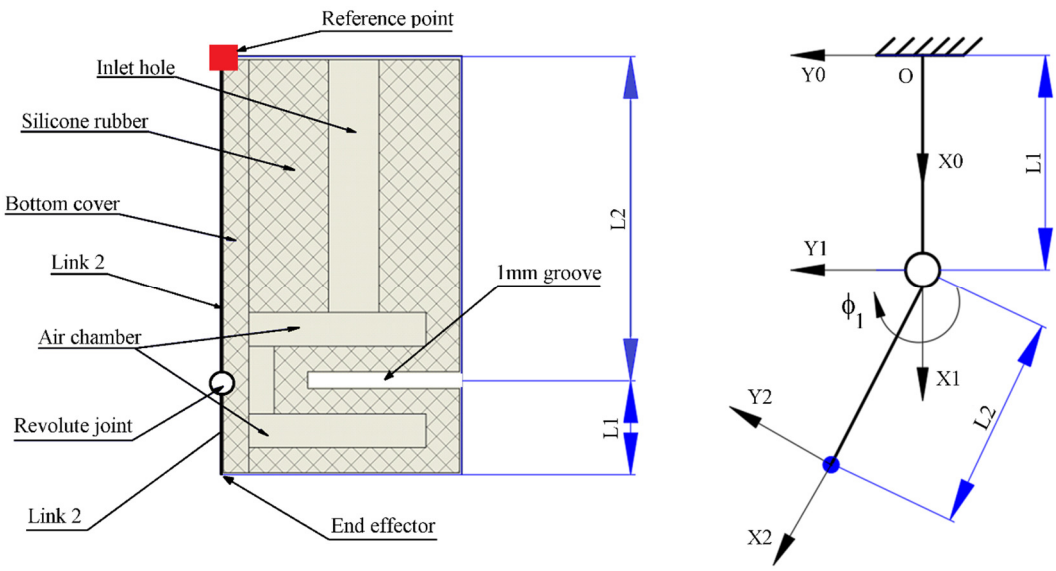

Fig. 11 2-air chamber actuator model

The end-effector of the actuator is defined by two simple geometric equations to calculate x and y displacements:

$$X2=L1+L2\times\cos\theta_1 \tag{3}$$

$$Y2=L2\times\sin\theta_1 \tag{4}$$

Eqs. (3)-(4) are straightforward to derive because this soft actuator has only two air chambers with one angle variable. However, when the number of serial links and joints in a robot increases, the task of solving the kinematics problem becomes increasingly complex due to a large number of joint variables. The DH method is widely used in robotics to describe the geometry of a serial-link mechanism. This provides a foundation for roboticists to apply algorithmic methods and obtain solutions for kinematic problems [17]. Therefore, the DH method is utilized to determine the motion of the robot. A soft robot model with serial links and finite joints is presented in Fig. 12.

By following these steps, the motion of a soft robot can be accurately described:

(1) Identify the number of joints in the robot. This will help in determining the number of joint variables required to describe the robot's motion: Depending on the air chamber quantities (n) in the robot, it has (n-1) revolute joints rotating around the z-axis, which are connected to (n) links.

(2) Determine the 4 DH parameters (θ, α, r, d) for each frame.

(3) Find the homogeneous transformation matrix of each frame using the DH parameters.

(4) Derive the transformation matrix for each frame by multiplying the corresponding matrices from frame 0 to frame n.

(5) Substitute the bending angle from the experimental data into the displacement vectors (X and Y) in the H_{n-1}^{n} matrices (n ≥ 1) to determine the position of each frame.

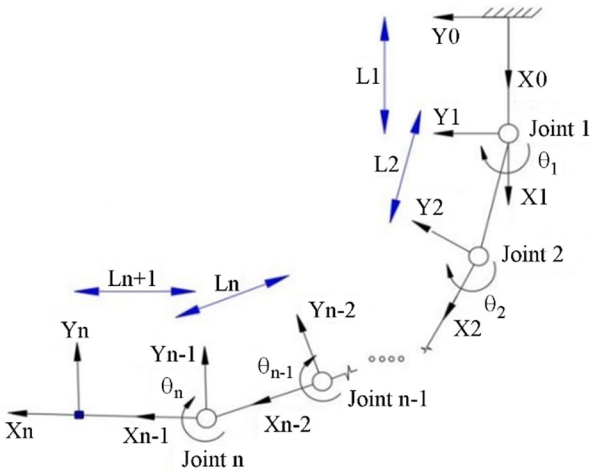

Fig. 12 The soft actuator model with serial links and rotational joints

The homogeneous transformation matrix for the nth frame can be expressed as:

$$H_{n-1}^{n} = \begin{vmatrix} \cos\theta_n & -\sin\theta_n\cos\alpha_n & \sin\theta_n\sin\alpha_n & r_n\cos\theta_n \\ \sin\theta_n & \cos\theta_n\cos\alpha_n & -\cos\theta_n\sin\alpha_n & r_n\sin\theta_n \\ 0 & \sin\alpha_n & \cos\alpha_n & d_n \\ 0 & 0 & 0 & 1 \end{vmatrix} \tag{5}$$

where θ = bending angle of X_n and X_{n+1}, α = bending angle of Z_n and Z_{n+1}, r = distance from X_n and X_{n+1}, measure along X_{n+1}, and d = distance from Z_n and Z_{n+1}, measure along Z_n.

Table 1 DH parameters

Joint	θ	α	r	d
1	θ_1	0	L_2	0
2	θ_2	0	L_3	0
⋮				
n	θ_n	0	L_{n+1}	0

Then, DH parameters in Table 1 are substituted into Eq. (5), which determines the displacements and orientations of each frame. After determining all the DH parameters, the DH matrices of all joints are multiplied by each other to obtain the overall homogeneous transformation matrix. It can be expressed as follows:

$$H_{0}^{n} = \begin{vmatrix} \cos\theta_1 & -\sin\theta_1 & 0 & L_1 + L_2\times\cos\theta_1 \\ \sin\theta_1 & \cos\theta_1 & 0 & L_2\times\sin\theta_1 \\ 0 & 0 & 1 & 0 \\ 0 & 0 & 0 & 1 \end{vmatrix} \cdots \begin{vmatrix} \cos\theta_n & -\sin\theta_n & 0 & L_n + L_{n+1}\times\cos\theta_n \\ \sin\theta_n & \cos\theta_n & 0 & L_{n+1}\times\sin\theta_n \\ 0 & 0 & 1 & 0 \\ 0 & 0 & 0 & 1 \end{vmatrix} \tag{6}$$

Eq. (6) provides the mathematical representation of the spatial relationship between the nth frame and the reference frame (frame 0) in terms of position and orientation. However, when a robot has numerous joints and links, resulting in a greater number of joint variables, the process of deriving the homogeneous transformation matrix for each frame becomes more complex. Consequently, for robots with more than two joint variables, the joint angle variables are represented by a single angle variable, with all angle variables assumed to be equal.

The uniform geometry of the robot air chambers results in a similar bending angle of two consecutive links. This assertion is supported by the experimental data gathered from the 4-air chamber and 6-air chamber actuators, which measured the bending angle of each joint. The bending motion of a soft actuator with n joints (i.e., n+1 air chambers) is then derived as:

$$X_n = L_1 + L_2 \times \cos\theta + L_3 \times \cos 2\theta + L_4 \times \cos 3\theta + \ldots + L_n \times \cos\theta_{n-1} + L_{n+1} \times \cos\theta_n \tag{7}$$

$$Y_n = L_2 \times \sin\theta + L_3 \times \sin 2\theta + L_4 \times \sin 3\theta + \ldots + L_n \times \sin\theta_{n-1} + L_{n+1} \times \sin\theta_n \tag{8}$$

In Eqs. (7)-(8), the variables X_n and Y_n represent the displacements of the nth frame with respect to the x and y displacements in the planar space. In the transformation matrix H_0^n, X_n, and Y_n correspond to the displacements of the nth frame with respect to the x and y displacements in the planar space. Specifically, X_n is in the first row and fourth column of the matrix, while Y_n is in the second row and fourth column.

The relationship between bending angle and air pressure can be expressed by:

$$\varphi = \frac{\left(-0.0036 \times P^2 + 0.6916 \times P\right) \times \pi}{180} \tag{9}$$

where φ denotes the bending angle (Radian) and P is the air pressure (KPa).

As shown in Fig. 13 and expressed in Eq. (9), polynomial interpolation is utilized in this study to predict the bending motion of various air chamber actuators. The compressed air variable substitutes the angle variable in the displacement matrices H_n^{XY}, where n is the ordinal of the rotational joint, to determine the position of the soft actuator. The transformation matrix is then utilized to visualize the motion of the soft actuator with the corresponding pressure values. Furthermore, Python programming language is used to plot and save the plot pictures with different pressure values automatically.

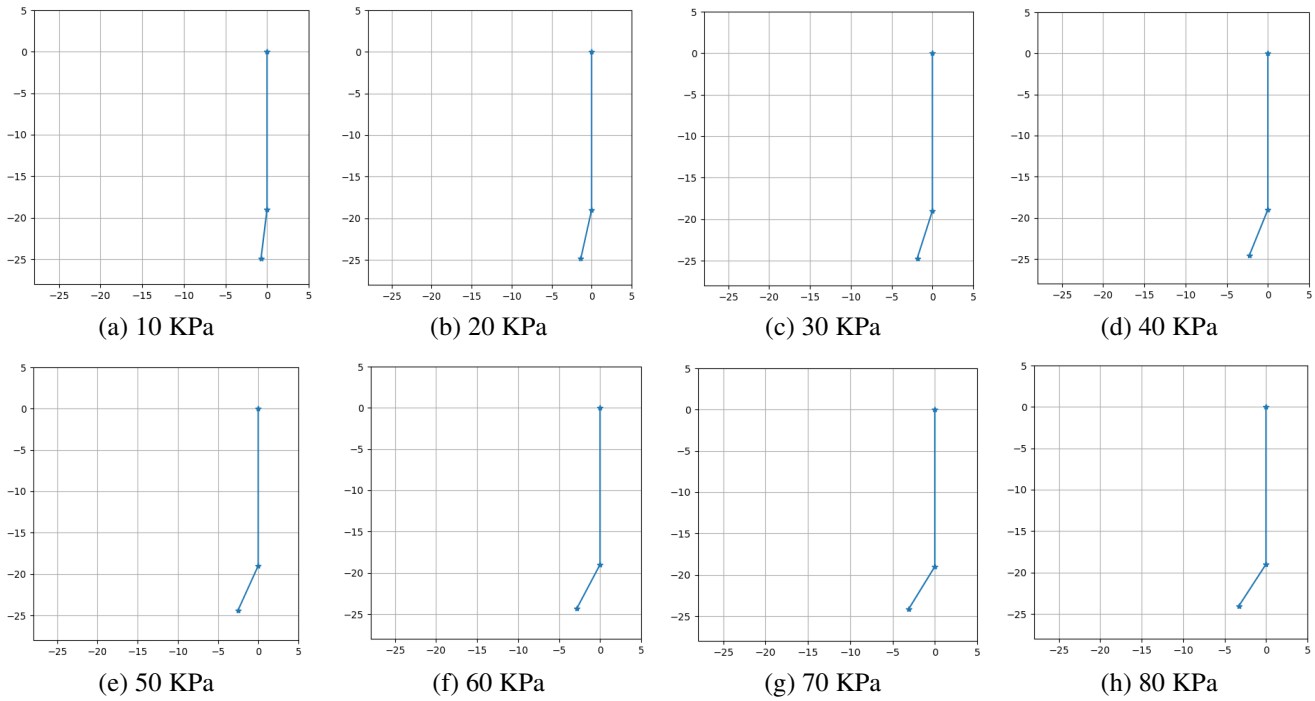

Fig. 13 The soft actuator graph of Eqs. (3)-(4), and (9)

6. Results and Discussion

According to Fig. 14, the predicted bending angle of the soft actuator with various air chambers is approximately the same as that of the 2-air chamber actuator, which is interpolated from the experimental data. Furthermore, it is observed that as the number of air chambers increases, the bending angle of each joint may decrease within the pressure range of 10-80 KPa. However, the accuracy of the prediction may be affected by Earth's gravitational force as the weight of the actuator increases with the addition of more air chambers. The approach to address this issue and improve the accuracy of the prediction will be presented in future work. The average bending angle is expressed as:

$$Bending_angle_n = \frac{Bending_angle_1 + Bending_angle_2 + \ldots + Bending_angle_n}{\mathrm{n}} \tag{10}$$

where n is the ordinal bending angle (n ≥ 2). If the actuator has n + 1 air chambers (links), it will have n bending angle (joints). Eq. (10) is utilized to compute the bending angle of the soft pneumatic actuator with various number of air chambers. It expresses the orientation between two adjacent air chambers.

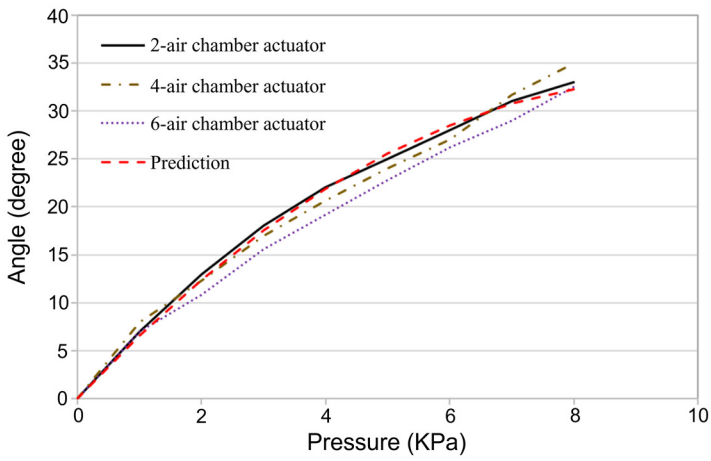

Fig. 14 Bending angle of the soft actuators

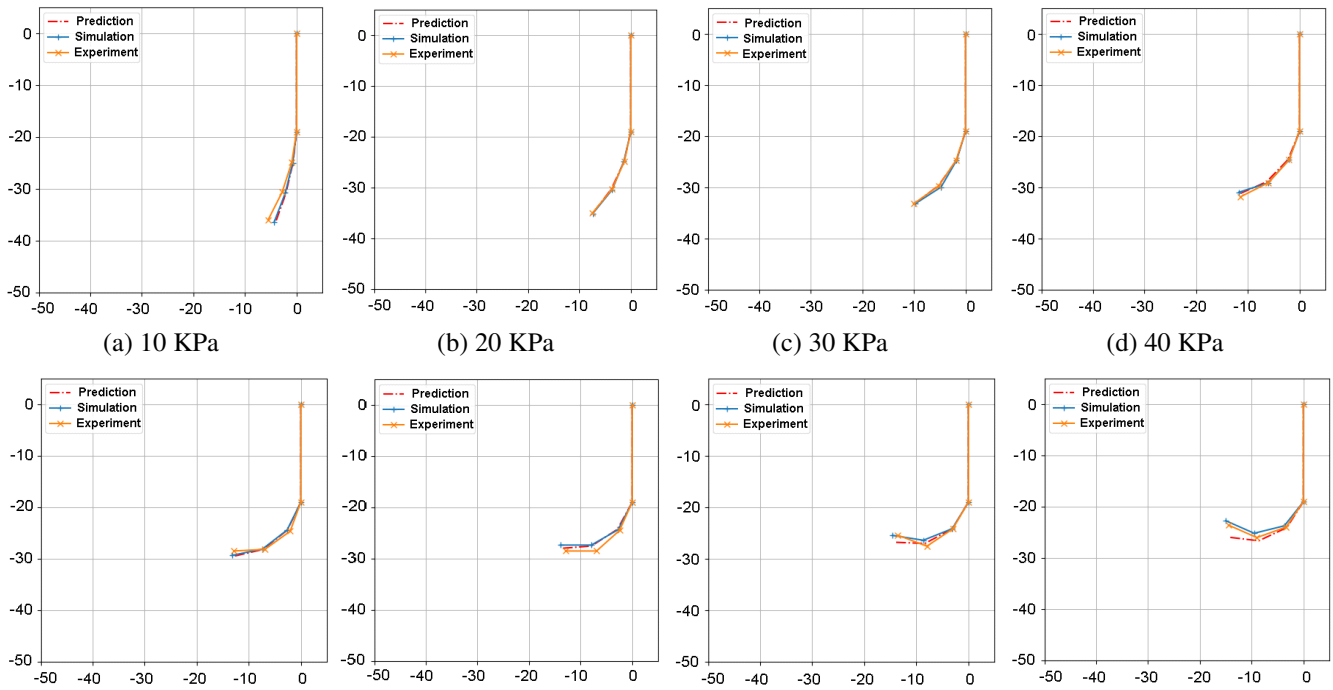

(a) 10 KPa (b) 20 KPa (c) 30 KPa (d) 40 KPa

(e) 50 KPa (f) 60 KPa (g) 70 KPa (h) 80 KPa

Fig. 15 Forward kinematics model of 4-air chamber actuator

Python was utilized to generate line graphs that simulate the position of the simulation, experiment, and predicted bending angle of the 4-air (Fig. 15) and 6-air (Fig. 16) chamber soft actuators. The experimental results indicate that the prediction using the 4-air chamber actuator is nearly identical to the experiment and simulation in the pressure range of 0 KPa to 70 KPa. However, with the 6-air chamber actuator, there is a slight difference between the prediction and the experimental test. The experiment sections of the 4-air and 6-air chamber actuators were compared. It was observed that as the number of air chambers increases, the bending angle decreases. This decrease in the bending angle is due to the increase in mass of the soft actuator as the number of air chambers increases, which partially reduces the strain angle.

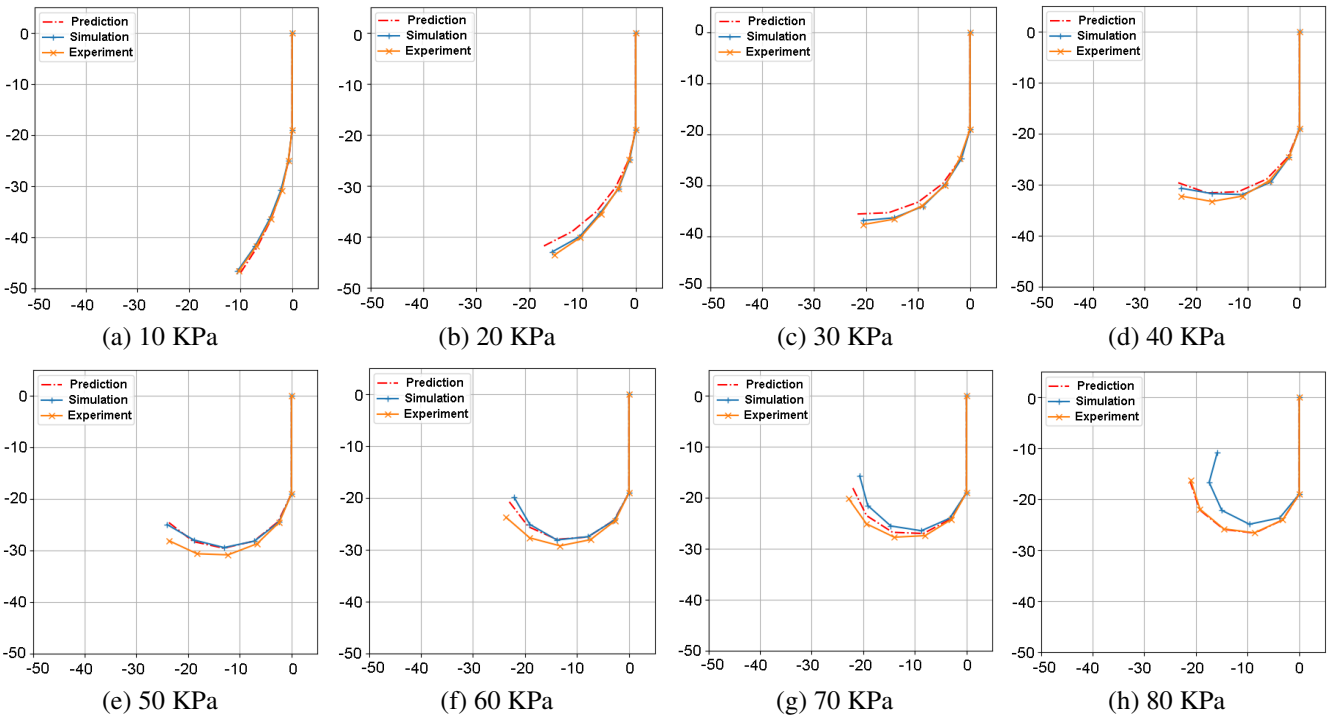

Fig. 16 Forward kinematics model of 6-air chamber actuator

7. Conclusions

The paper presented the design, simulation, and fabrication processes, as well as the FK model of soft pneumatic actuators with different numbers of air chambers. The actuators and the molds were fabricated by using casting with silicone rubber and 3D printing technology, respectively. The investigation involves 2-air, 4-air, and 6-air chamber soft pneumatic actuators, and an experiment was conducted to measure the bending angle of these actuators. Before making the actuators, a simulation of the stress-strain behavior of the soft robot was executed to optimize the design using Ansys software. The FK model of the 4-air and 6-air chamber actuators is developed based on the angle data of the 2-air chamber actuator.

The results show that acceptable bending angles are within a 5% tolerance. By using the experimental data of the 2-air chamber actuator combined with the FK model, the bending motion of the 4-air and 6-air chamber actuators can be predicted accurately with an acceptable error rate under 10% for the simulation, experiment, and FK model. However, an actuator with a greater number of air chambers can cause an error in the prediction due to its heavier weight. A constant need to be added after the equation of bending angle and pressure, and it will take a lot of experiments with various actuators to determine the constant. In future work, how to determine the constant caused by the weight of the actuators will be investigated.

Acknowledgment

The support of time and facilities from Ho Chi Minh City University of Technology (HCMUT), VNU– HCM for this study are acknowledged.

Conflicts of Interest

The authors declare no conflict of interest.

References

[1] P. H. Le, T. P. Do, and D. B. Le, "A Soft Pneumatic Finger with Different Patterned Profile," International Journal of Mechanical Engineering and Robotics Research, vol. 10, no. 10, pp. 577-582, October 2021.

[2] H. Marvi, G. Z. Lum, and I. D. Walker, "Opportunities and Challenges in Soft Robotics," Advanced Intelligent Systems, vol. 2, no. 6, June 2020.

[3] P. T. Do, D. T. Vo, and H. P. Le, "A Soft Pneumatic Robotic Glove for Hand Rehabilitation after Stroke," 20th International Conference on Advanced Robotics, pp. 7-12, January 2022.

[4] M. Xie, M. Zhu, Z. Yang, S. Okada, and S. Kawamura, "Flexible Self-Powered Multifunctional Sensor For Stiffness-Tunable Soft Robotic Gripper by Multimaterial 3D Printing," Nano Energy, vol. 79, article no. 105438, January 2021.

[5] Z. Wang, T. Hirata, T. Sato, T. Mori, M. Kawakami, H. Furukawa, et al., "A Soft Robotic Hand Based on Bellows Actuators for Dishwashing Automation," IEEE Robotics and Automation Letters, vol. 6, no. 2, pp. 2139-2146, April 2021.

[6] L. Xiaohui, Z. Liping, and Z. Wei, "Hook-Shaped Bending and S-Shaped Bending of Soft Robotic Arm," 4th International Conference on Robotics and Automation Sciences, pp. 1-5, June 2020.

[7] H. Wang, M. Totaro, and L. Beccai, "Toward Perceptive Soft Robots: Progress and Challenges," Advanced Science, vol. 5, no. 9, September 2018.

[8] Z. Wang, K. Or, and S. Hirai, "A Dual-Mode Soft Gripper for Food Packaging," Robotics and Autonomous Systems, vol. 125, article no. 103427, March 2020.

[9] M. T. Thai, P. T. Phan, T. T. Hoang, H. Low, N. H. Lovell, and T. N. Do, "Design, Fabrication, and Hysteresis Modeling of Soft Microtubule Artificial Muscle (SMAM) for Medical Applications," IEEE Robotics and Automation Letters, vol. 6, no. 3, pp. 5089-5096, July 2021.

[10] Z. Wang and S. Hirai, "Soft Gripper Dynamics Using a Line-Segment Model with an Optimization-Based Parameter Identification Method," IEEE Robotics and Automation Letters, vol. 2, no. 2, pp. 624-631, April 2017.

[11] H. Al-Fahaam, S. Davis, and S. Nefti-Meziani, "The Design and Mathematical Modelling of Novel Extensor Bending Pneumatic Artificial Muscles (EBPAMS) for Soft Exoskeletons," Robotics and Autonomous Systems, vol. 99, pp. 63-74, January 2018.

[12] S. Luo, M. Edmonds, J. Yi, X. Zhou, and Y. Shen, "Spline-Based Modeling and Control of Soft Robots," IEEE/ASME International Conference on Advanced Intelligent Mechatronics, pp. 482-487, July 2020.

[13] M. E. M. Salem, Q. Wang, and M. H. Xu, "Application of Neural Network Fitting for Modeling the Pneumatic Networks Bending Soft Actuator Behavior," Engineering Research Express, vol. 4, no. 1, article no. 15032, March 2022.

[14] C. R. Rocha, C. P. Tonetto, and A. Dias, "A Comparison Between the Denavit–Hartenberg and The Screw-Based Methods Used in Kinematic Modeling of Robot Manipulators," Robotics and Computer-Integrated Manufacturing, vol. 27, no. 4, pp. 723-728, August 2011.

[15] C. Faria, J. L. Vilaca, S. Monteiro, W. Erlhagen, and E. Bicho, "Automatic Denavit-Hartenberg Parameter Identification for Serial Manipulators," 45th Annual Conference of the IEEE Industrial Electronics Society, pp. 610-617, October 2019.

[16] I. M. Meththananda, S. Parker, M. P. Patel, and M. Braden, "The Relationship Between Shore Hardness of Elastomeric Dental Materials and Young's Modulus," Dental Materials, vol. 25, no. 8, pp. 956-959, August 2009.

[17] P. I. Corke, "A Simple and Systematic Approach to Assigning Denavit–Hartenberg Parameters," IEEE Transactions on Robotics, vol. 23, no. 3, pp. 590-594, June 2007.

Copyright© by the authors. Licensee TAETI, Taiwan. This article is an open access article distributed under the terms and conditions of the Creative Commons Attribution (CCBY) license (http://creativecommons.org/licenses/by/4.0/).